Simulating quantum state engineering in spontaneous parametric down-conversion using classical light

Yingwen Zhang,[1] Melanie Mclaren,[1] Filippus S. Roux,[1] and Andrew Forbes[1,2,*]

[1]*CSIR National Laser Centre, PO Box 395, Pretoria 0001, South Africa*
[2]*School of Chemistry and Physics, University of KwaZulu-Natal, Private Bag X54001, 4000 Durban, South Africa*

[*]*AForbes1@csir.co.za*

Abstract: We present a simple method of simulating the effect of the pumping process in spontaneous parametric down-conversion (SPDC) by modulating a classical laser beam with two spatial light modulators through a back projection setup. We simulate a wide range of pump beams for quantum state engineering and confirm that the results are in agreement with theory. Our approach offers high photon count rates, is quick to yield results and can easily be converted back to a SPDC setup. It is likely to be a useful tool before starting more complicated SPDC experiments with custom pump profiles.

OCIS codes: (140.3300) Laser beam shaping; (190.4410) Nonlinear optics, parametric processes; (270.0270) Quantum optics; (070.6120) Spatial light modulators.

References and links

1. M. A. Nielsen, and I. L. Chuang, *Quantum Computation and Quantum Information* (Cambridge University, 2010).
2. G. Molina-Terriza, J. P. Torres, and L. Torner, "Twisted photons," Nat. Phys. **3,** 305–310 (2007).
3. B. Jack, A. M. Yao, J. Leach, J. Romero, S. Franke-Arnold, D. G. Ireland, S. M. Barnett, and M. J. Padgett, "Entanglement of arbitrary superpositions of modes within two-dimensional orbital angular momentum state spaces," Phys. Rev. A **81,** 043844 (2010).
4. J. Leach, B. Jack, J. Romero, A. Jha, A. M. Yao, S. Franke-Arnold, D. G. Ireland, R. W. Boyd, S. M. Barnett, and M. J. Padgett, "Quantum correlations in optical angleorbital angular momentum variables," Science **329,** 662–665 (2010).
5. A. Aiello, S. S. R. Oemrawsingh, E. R. Eliel, and J. P. Woerdman, "Nonlocality of high-dimensional two-photon orbital angular momentum states," Phys. Rev. A **72,** 052114 (2005).
6. J. Romero, J. Leach, B. Jack, S. M. Barnett, M. J. Padgett, and S. Franke-Arnold, "Violation of Leggett inequalities in orbital angular momentum subspaces," New J. Phys. **12**, 123007 (2010).
7. L. Chen, and J. Romero, "Hardy's nonlocality proof using twisted photons," Opt. Express **20**, 21687–21692 (2012).
8. E. Karimi, F. Cardano, M. Maffei, C. de Lisio, L. Marrucci, R. Boyd, and E. Santamato, "Hardy's paradox tested in the spin-orbit hilbert space of single photons," Phys. Rev. A **89**, 032122 (2014).
9. A. Mair, A. Vaziri and G. Weihs, and A. Zeilinger, "Entanglement of the orbital angular momentum states of photons," Nature (London) **412,** 313–316 (2001).
10. M. Agnew, J. Leach, M. McLaren, F. Roux, and R. Boyd, "Tomography of the quantum state of photons entangled in high dimensions," Phys. Rev. A **84**, 062101 (2011).
11. M. McLaren, M. Agnew, J. Leach, F. Roux, M. Padgett, R. Boyd, and A. Forbes, "Entangled Bessel-Gaussian beams," Opt. Express **20**, 23589–23597 (2012).

#211382 - $15.00 USD Received 2 May 2014; revised 21 Jun 2014; accepted 23 Jun 2014; published 3 Jul 2014

12. M. Mclaren, J. Romero, M. J. Padgett, and A. Forbes, "Two-photon optics of Bessel-Gaussian modes," Phys. Rev. A **88,** 033818 (2013).
13. M. Mclaren, T. Mhlanga, M. J. Padgett, F. S. Roux, and A. Forbes, "Self-healing of quantum entanglement after an obstruction," Nature Commun. **5,** 3248 (2014).
14. M. Krenn, R. Fickler, M. Huber, R. Lapkiewicz, W. Plick, S. Ramelow, and A. Zeilinger, "Entangled singularity patterns of photons in Ince-gauss modes," Phys. Rev. A **87**, 012326 (2013).
15. H. Di Lorenzo Pires, H. Florijn, and M. van Exter, "Measurement of the spiral spectrum of entangled two-photon states," Phys. Rev. Lett. **104**, 020505 (2010).
16. J. Romero, D. Giovannini, S. Franke-Arnold, S. M. Barnett, and M. J. Padgett, "Increasing the dimension in high-dimensional two-photon orbital angular momentum entanglement," Phys. Rev. A **86**, 012334 (2012).
17. J. Barreiro, N. Langford, N. Peters, and P. Kwiat, "Generation of hyper-entangled photon pairs," Phys. Rev. Lett. **95**, 260501 (2005).
18. M. Malik, M. Mirhosseini, M. Lavery, J. Leach, M. Padgett, and R. Boyd, "Direct measurement of a 27-dimensional orbital-angular-momentum state vector," Nature Commun. **5**, 3115 (2014).
19. R. Fickler, R. Lapkiewicz, M. Huber, M. Lavery, M. Padgett, and A. Zeilinger, "Interface between path and OAM entanglement for high-dimensional photonic quantum information," arXiv:1402.2423v2 (2014).
20. D. Giovannini, J. Romero, J. Leach, A. Dudley, A. Forbes, and M. J. Padgett, "Characterization of high-dimensional entangled systems via mutually unbiased measurements," Phys. Rev. Lett. **110**, 143601 (2013).
21. M. Mafu, A. Dudley, S. Goyal, D. Giovannini, M. Mclaren, M. J. Padgett, T. Konrad, F. Petruccione, N. Lutkenhaus and A. Forbes, "Higher-dimensional orbital-angular-momentum-based quantum key distribution with mutually unbiased bases," Phys. Rev. A **88**, 032305 (2013).
22. B. Lanyon, M. Barbieri, M. Almeida, T. Jennewein, T. Ralph, K. Resch, G. Pryde, J. O'Brien, A. Gilchrist, and A. White, "Simplifying quantum logic using higher-dimensional Hilbert spaces," Nature Physics **5**, 134–140 (2009).
23. M. Cardano, F. Francesco, E. Karimi, S. Slussarenko, D. Paparo, C. de Lisio, F. Sciarrino, E. Santamato, and L. Marrucci, "Photonic quantum walk in a single beam with twisted light," arXiv:1403.4857v1 (2014).
24. K. Goyal and T. Konrad, "Teleporting photonic qudits using multimode quantum scissors," Scientific Reports **3**, 3548 (2013).
25. S. Franke-Arnold, S. M. Barnett, M. J. Padgett, and L. Allen, "Two-photon entanglement of orbital angular momentum states," Phys. Rev. A **65,** 033823 (2002).
26. J. P. Torres, A. Alexandrescu, and L. Torner, "Quantum spiral bandwidth of entangled two-photon states," Phys. Rev. A **68,** 050301 (2003).
27. E. J. S. Fonseca, C. H. Monken, and S. Pádua, "Measurement of the de Broglie wavelength of a multiphoton wave packet," Phys. Rev. Lett. **82,** 2868 (1999).
28. S. P. Walborn, A. N. de Oliveira, R. S. Thebaldi, and C. H. Monken, "Entanglement and conservation of orbital angular momentum in spontaneous parametric down-conversion," Phys. Rev. A **69,** 023811 (2004).
29. T. Yarnall, A. F. Abouraddy, B. E. A. Saleh, and M. C. Teich, "Experimental violation of Bells inequality in spatial-parity space," Phys. Rev. Lett. **99,** 170408 (2007).
30. T. Yarnall, A. F. Abouraddy, B. E. A. Saleh, and M. C. Teich, "Synthesis and analysis of entangled photonic qubits in spatial-parity space," Phys. Rev. Lett. **99,** 250502 (2007).
31. R. M. Gomes, A. Salles, F. Toscano, P. H. Souto Ribeiro, and S. P. Walborn, "Observation of a nonlocal optical vortex," Phys. Rev. Lett. **103,** 033602 (2009).
32. J. Romero, D. Giovannini, M. G. Mclaren, E. J. Galvez, A. Forbes, and M. J. Padgett, "Orbital angular momentum correlations with a phase-flipped Gaussian mode pump beam," J. Opt. **14,** 085401 (2012).
33. D. Klyshko, "A simple method of preparing pure states of an optical field, of implementing the EinsteinPodolskyRosen experiment, and of demonstrating the complementarity principle," Sov. Phys. Usp. **31,** 74 (1988)
34. R. S. Aspden, D. S. Tasca, A. Forbes, R. W. Boyd and M. J. Padgett, "Experimental demonstration of Klyshkos advanced-wave picture using a coincidence-count based, camera-enabled imaging system," J. Mod. Opt. 10.1080/09500340.2014.899645 (2014).
35. F. M. Miatto, A. M. Yao, and S. M. Barnett, "Full characterization of the quantum spiral bandwidth of entangled biphotons," Phys. Rev. A **83,** 033816 (2011).
36. Y. Zhang, and F. S. Roux, "Modal spectrum in spontaneous parametric down-conversion with noncollinear phase matching," Phys. Rev. A **89,** 063802 (2014).
37. Y. Zhang, F. S. Roux, M. Mclaren, and A. Forbes, "Radial modal dependence of the azimuthal spectrum after parametric down-conversion," Phys. Rev. A **89,** 043820 (2014).
38. V. Arrizón, U. Ruiz, R. Carrada, and L. A. González, "Pixelated phase computer holograms for the accurate encoding of scalar complex fields," J. Opt. Soc. Am. A **24,** 3500–3507 (2007).
39. T. Ando, Y. Ohtake, N. Matsumoto, T. Inoue, and N. Fukuchi, "Mode purities of LaguerreGaussian beams generated via complex-amplitude modulation using phase-only spatial light modulators," Opt. Lett. **34,** 34–36 (2009)

#211382 - $15.00 USD Received 2 May 2014; revised 21 Jun 2014; accepted 23 Jun 2014; published 3 Jul 2014

1. Introduction

Entanglement is a distinct phenomenon of quantum mechanics. A proper understanding and use of entanglement can lead to significant technological advances in communication, computing and cryptography [1]. In recent years there has been much interest in the entanglement among optical modes that carry orbital angular momentum (OAM) [2]. These modes are capable of carrying large amounts of information due to the infinite-dimensional nature of OAM and thus are of significant interest for quantum information. They have been used to demonstrate the violation of Bell's inequality [3–5] and Leggett inequalities [6] as well as demonstrating Hardy's paradox [7,8]. Typically, OAM carrying modes such as Laguerre-Gaussian (LG) [9,10], Bessel-Gaussian [11–13] and Ince-Gaussian [14] have been used to demonstrate high-dimensional entanglement. An increase in the dimensionality of an entangled system offers an increase in information capacity per photon. As such, a variety of work, from increasing the measured spiral bandwidth [15,16] to increasing the number of entangled degrees of freedom [17], has been experimentally demonstrated. Alternatively, the direct measurement technique has shown entanglement up to 27 dimensions using both weak and strong measurements [18]. More recently, high-dimensional spatial entanglement was achieved by transferring the dimensionality of path entangled photons to the OAM degree of freedom [19]. The advantages of high-dimensional entanglement include an increased tolerance to eavesdropping in quantum key distribution [20,21] as well as an increased efficiency in computing logic gates in quantum computation [22]. The potential for high-dimensional entanglement with OAM modes has been used to show a quantum random walk up to 4 steps [23] and has been proposed to demonstrate high-dimensional teleportation [24].

Such entangled states are routinely created in the laboratory by spontaneous parametric down-conversion (SPDC) [9, 25, 26], where the states are post selected with spatial light modulators. To date there have been very few studies making use of quantum states that have been prepared at the source by modulating the pump profile. In [9] where entanglement of photons in OAM states was first demonstrated, $\mathrm{LG}_0^{0,\pm1}$ modes were used in the pump beam. In [27], the pump profile was modified by placing a wire in its path to measure the de Broglie wavelength of a multiphoton packet. The coincidence profile of pump beams in the $\mathrm{LG}_0^{1,2}$ modes was measured and compared to theory in [28], while in [29, 30] Bell's measurement were performed on pump beams with modified spatial parity. Nonlocal optical vortices were observed in [31] where pump beams in the HG_{01} and $\mathrm{LG}_0^{\pm1}$ were used, and in [32] the OAM and angular position correlations of a HG_{01} pump was measured. The dearth of such experiments is likely due to the prohibitive cost and time, requiring custom optics likely resulting in low count rates. Consequently, quantum state engineering is largely restricted to post selection processes.

Inspired by the advanced-wave representation of Klyshko [33], it has recently been shown that back projection with classical light can mimic the *post* selection of modes in a SPDC experiment [12, 34]. In this paper we show that the Klyshko concept may be extended to include the pump beam too, the first time this is suggested, so that the effect of both *pre* and *post* selection of modes may be simulated. The advantage of this is that the tool becomes complete for the testing of quantum state engineering approaches. We modulate a classical laser beam with two spatial light modulators (SLM) where both the pump beam and down-converted beam profiles to be generated are encoded on the SLMs. The advantage of such a setup is that the photon count rate is many orders of magnitude larger than in a typical SPDC experiment resulting in better photon statistics and easier alignment. We show that the effect of using different pumps on the OAM spectrum can be investigated simply by reprogramming the SLMs with the corresponding pump profile. This can be used to give an indication of whether a SPDC experiment with a novel pump beam will be feasible or not. The back projection setup can also be easily converted into a SPDC setup by replacing just two of its components. We compute

#211382 - $15.00 USD Received 2 May 2014; revised 21 Jun 2014; accepted 23 Jun 2014; published 3 Jul 2014

theoretically the effect of Laguerre-Gaussian, Hermite-Gaussian and flat-top pump profiles and show experimental results consistent with the predictions. This approach will be useful tool in the engineering of entangled quantum states.

2. Coincidence amplitude of SPDC

The coincidence counts in a SPDC experiment are proportional to the modulus square of the down-converted probability amplitude, $|\mathscr{M}|^2 = |\langle \Psi_f | \mathscr{P} | \Psi_{in} \rangle|^2$, where $\mathscr{P}$ represents the SPDC process and Ψ_{in} and Ψ_f are the initial and final photon states, respectively. For type I phase matching, with collinear signal and idler beams and degenerate signal and idler frequencies ($\omega_s = \omega_i = \frac{1}{2}\omega_p$), the probability amplitude in the paraxial limit is given by the overlap integral [35, 36]:

$$\mathscr{M} = \Omega_0 \int M_s^*(\mathbf{q}_s) M_i^*(\mathbf{q}_i) M_p(\mathbf{q}_s + \mathbf{q}_i) S(\mathbf{q}_s - \mathbf{q}_i) \frac{\mathrm{d}^2 q_s}{(2\pi)^2} \frac{\mathrm{d}^2 q_i}{(2\pi)^2} \tag{1}$$

where Ω_0 is an overall constant that determines the conversion efficiency, $\mathbf{q} = q_x \hat{x} + q_y \hat{y}$ is the two-dimensional transverse part of the three-dimensional wave-vector $\mathbf{k}$, the angular spectra of the mode profiles of the signal, idler and pump beams are given by $M_s(\mathbf{q})$, $M_i(\mathbf{q})$ and $M_p(\mathbf{q})$, respectively, and $S(\mathbf{q}_s - \mathbf{q}_i)$ is the phase matching function.

In the case of collinear signal and idler beams the phase matching function is given by [35, 36]:

$$S(\mathbf{q}_s - \mathbf{q}_i) = \mathrm{sinc}\left(\frac{n_o L w_p^2}{8 z_R} |\mathbf{q}_s - \mathbf{q}_i|^2 \right), \tag{2}$$

where we define $\mathrm{sinc}(a) = \sin(a)/a$ with n_o the ordinary refractive index of the nonlinear crystal, L is the crystal length and z_R is the Rayleigh range of the pump beam. In most typical SPDC experiments $L \ll z_R$ and in this limit the phase matching function can simply be approximated by unity. As a result, one can Fourier transform Eq. (1) [37] to the coordinate domain which gives

$$\mathscr{M} = \Omega_0 \int m_p(\mathbf{x}) m_s^*(\mathbf{x}) m_i^*(\mathbf{x}) \, \mathrm{d}^2 x, \tag{3}$$

where $m_{p,s,i}(\mathbf{x})$ represents the mode profile of the pump, signal or idler beam.

In a conventional SPDC experiment $m_s(\mathbf{x})$ and $m_i(\mathbf{x})$ are each encoded on a SLM to select the signal and idler modes to be detected, while the pump mode, $m_p(x)$, is the standard output from the pump source, a Gaussian function. Here we show that a classical system described by the same integral Eq. (3) can be produced by also encoding $m_p(\mathbf{x})$ onto the SLMs allowing pre- and post-selection mode experiments to be done with a classical laser beam and only two SLMs.

In this paper three different pump beam types are simulated. The first is a pump beam with a vortex beam profile where

$$m_p^\ell(\mathbf{x}) = \frac{1}{w_p} \left(\frac{2^{|\ell_p|}}{|\ell_p|!} \right)^{1/2} \left(\frac{r}{w_p} \right)^{|\ell_p|} \exp\left(-\frac{r^2}{w_p^2} \right) \exp(i \ell_p \phi), \tag{4}$$

with w_p being the radius of the pump beam waist and ℓ_p the azimuthal index of the pump.

Secondly, we introduce a flat-top beam

$$m_p(\mathbf{x}) = \begin{cases} \frac{1}{\sqrt{\pi} w_p} & \text{for} \quad r < w_p \\ 0 & \text{for} \quad r > w_p \end{cases}, \tag{5}$$

#211382 - $15.00 USD Received 2 May 2014; revised 21 Jun 2014; accepted 23 Jun 2014; published 3 Jul 2014

and lastly we employ a Hermite Gaussian (HG) pump beam

$$m_p^{m,n}(\mathbf{x}) = \frac{1}{w_p}\left(\frac{1}{2^{n+m}n!m!}\right)^{1/2}\exp\left(-\frac{x^2+y^2}{w_p^2}\right)H_n\left(\frac{\sqrt{2}x}{w_p}\right)H_m\left(\frac{\sqrt{2}y}{w_p}\right), \tag{6}$$

where $H_{n,m}(x)$ are the Hermite polynomials of order n and m respectively.

LG modes are used for the signal and idler beam profiles and are given by

$$m_{s,i}^{\ell,p}(\mathbf{q}) = \frac{1}{w}\left[\frac{2^{|\ell|}p!}{(p+|\ell|)!}\right]^{1/2}\left(\frac{r}{w}\right)^{|\ell|}\exp\left(-\frac{r^2}{w^2}\right)L_p^{|\ell|}\left(\frac{2r^2}{w^2}\right)\exp(i\ell\phi), \tag{7}$$

where w is the radius of the beam waists and $L_p^{|\ell|}(x)$ is the generalized Laguerre polynomial with radial index p and azimuthal index ℓ. For simplicity we assume that the radii of the beam waists of the signal and idler beams are equal $w_s = w_i = w$.

Equation (3) shall then be solved numerically using the beam profiles Eq. (4-7) and compared to experiment.

3. Experimental concept and setup

The back-projection setup is inspired by the advanced-wave representation of Klyshko [33]. The Klyshko picture shows that the probability of detecting a photon in detector B given that another photon is detected in detector A is the same as if a photon propagates in reverse from detector A back to the crystal plane and is reflected through the system to detector B. The typical back-projection setup is just applying the Klyshko picture experimentally where one of the detectors is replaced by a laser source.

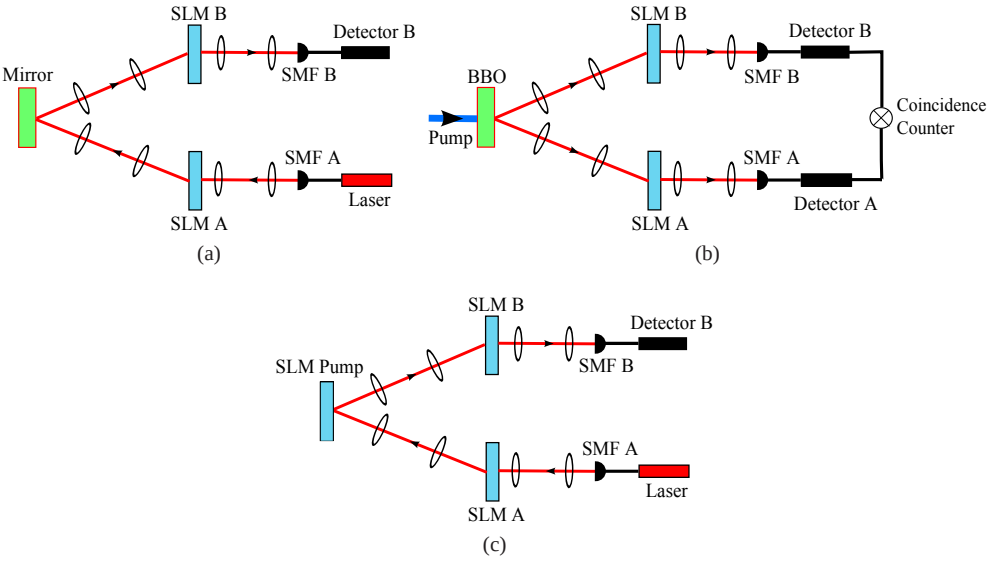

Fig. 1. Schematic diagram of a typical back-projection setup (a) compared to that of a SPDC setup (b). Back-projection setup to simulate the pump profile is shown in (c) where the mirror in (a) is replaced by a SLM.

A schematic of a typical back-projection setup is shown in Fig. 1(a) with the corresponding SPDC experiment in Fig. 1(b). An obvious difference is that the pump beam from the SPDC

#211382 - $15.00 USD Received 2 May 2014; revised 21 Jun 2014; accepted 23 Jun 2014; published 3 Jul 2014

experiment is not incorporated in any way. This leads to the overlap between the pump and the modes to be detected to be ignored, and moreover, and does not allow for pre-selection of quantum states to be simulated. We overcome these disadvantages by conceptionally replacing the pump beam and BBO crystal not with a mirror but with a third SLM, as seen in Fig. 1(c). In this way the pump beam is programmed as an appropriate hologram on the SLM, so that we realise a true simulation of Eq. (3). An important aspect of the SPDC experiment is that the planes of the crystal and SLMs are all image planes. As such, in the back-projection experiment the field at SLM A is relay imaged to the mirror (BBO crystal), and then relay imaged to SLM B. As a result the final field after SLM B is the overlap of the modes programmed on SLM A and B. To include the effect of the pump we have imagined an additional SLM in the place of the BBO crystal. For convenience we split the pump effect across the two existing SLMs (A and B) taking care of the imaging magnification. As one can see in the schematics in Fig. 1, the back-projection setup can be easily converted to the SPDC setup by replacing the mirror with a BBO crystal and replacing the laser with another avalanche photodiode (APD). Coincidence counts of the photon pairs can then be registered by a coincidence counter attached to the APDs.

In our setup a 710 nm laser beam was first coupled into a single mode fibre (SMF) A. The beam was then imaged onto SLM A via a telescope. SLM A was encoded to convert the Gaussian beam from the SMF into $\sqrt{m_p(\mathbf{x})}m_s^*(\mathbf{x})$. The beam was then imaged onto a mirror and was reflected onto SLM B with $\sqrt{m_p(\mathbf{x})}m_i^*(\mathbf{x})$ encoded. Finally the beam was coupled into SMF B which was connected to an APD that registers the photon counts. The type-3 intensity masking technique detailed in [38] was used to generate the hologram on the SLMs. The LG mode size w and the pump mode size w_p encoded on the hologram was 0.250 mm and the beam size of the Gaussian mode from the SMF when imaged onto the SLM was 0.575 mm.

4. Encoding the SLM

A slight complication in both back projection and SPDC experiments is that the beam emerging and coupling into the SMFs must be Gaussian beams; when this is taken into account the overlap integral to describe the back-projection setup becomes [37]

$$\mathscr{M} = \Omega_0 \int m_p(\mathbf{x}) m_s^*(\mathbf{x}) m_i^*(\mathbf{x}) G^2(\mathbf{x})\, \mathrm{d}^2x, \tag{8}$$

where

$$G(\mathbf{x}) = \left(\frac{2}{\pi}\right)^{1/2} \frac{1}{w_0} \exp\left(-\frac{x^2+y^2}{w_0^2}\right) \tag{9}$$

is the mode of the SMF, with radius w_0 when imaged onto the SLMs. It is mentioned in the experimental setup that $w_0 = 0.575$ mm for this experiment.

The effect of $G^2(\mathbf{x})$ has to be cancelled and this can be done by modifying the encoded functions on the SLMs. We can do this by modifying Eq.(7) into

$$m_{s,i}^{\ell,p}(\mathbf{q}) = \frac{1}{w}\left[\frac{2^{|\ell|}p!}{(p+|\ell|)!}\right]^{1/2} \left(\frac{r}{w}\right)^{|\ell|} \exp\left(-\frac{r^2}{(w')^2}\right) L_p^{|\ell|}\left(\frac{2r^2}{w^2}\right) \exp(i\ell\phi), \tag{10}$$

where

$$\frac{1}{(w')^2} = \frac{1}{w^2} - \frac{1}{w_0^2}. \tag{11}$$

We see that when using Eq. (10) in Eq. (8) we obtain the desired Eq. (3) for our overlap integral.

One other thing to take note when using this modification is in choosing the size of w. To demonstrate how the size of w can affect the beam quality we show in Fig. 2 the holograms

#211382 - $15.00 USD Received 2 May 2014; revised 21 Jun 2014; accepted 23 Jun 2014; published 3 Jul 2014

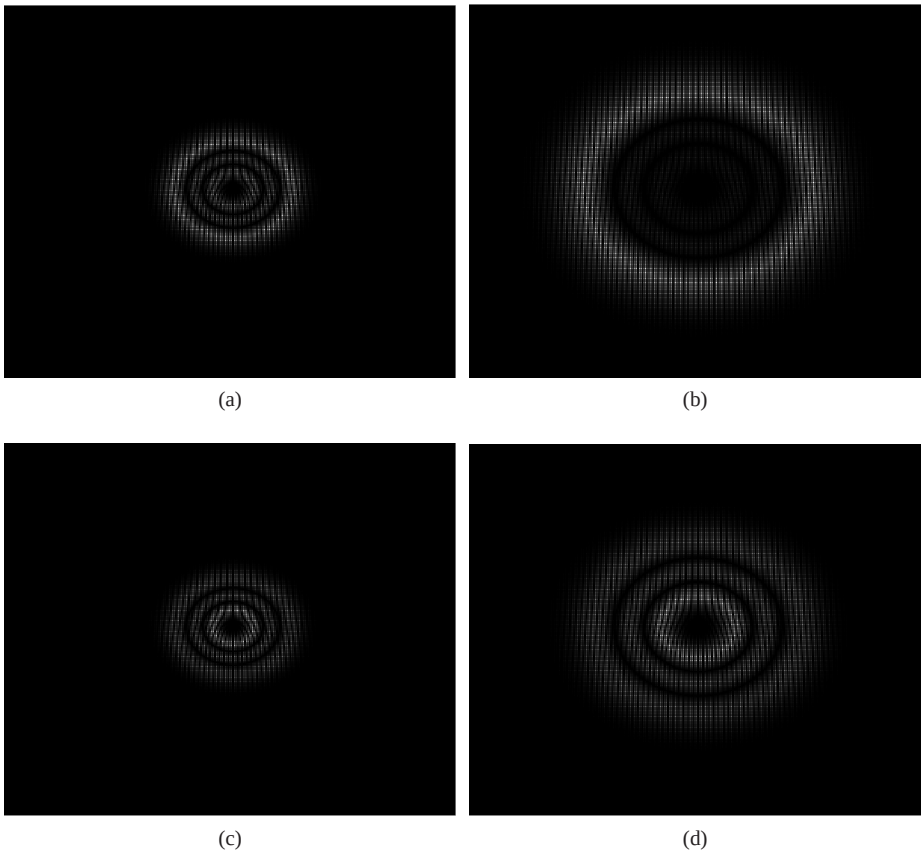

Fig. 2. Generated hologram on the SLM with $\sqrt{m_p(\mathbf{x})}m^*_{i,s}(\mathbf{x})$ encoded for a flat-top pump and LG signal and idler modes with $p = 2$, $\ell = 4$. (a) and (b) uses Eq.(10) as $m^*_{i,s}(\mathbf{x})$ with $w = w_p = 0.250$ mm for (a) and $w = w_p = 0.450$ mm for (b). (c) and (d) uses Eq.(7) as $m^*_{i,s}(\mathbf{x})$ with $w = w_p = 0.250$ mm for (c) and $w = w_p = 0.450$ mm for (d).

generated on the SLM with $\sqrt{m_p(\mathbf{x})}m^*_{i,s}(\mathbf{x})$ encoded for a flat-top pump and LG signal and idler modes with $p = 2$, $\ell = 4$. Figures 2(a) and 2(b) uses Eq. (10) as $m^*_{i,s}(\mathbf{x})$ with $w = w_p = 0.250$ mm for (a) and $w = w_p = 0.450$ mm for (b). Figures 2(c) and 2(d) shows the desired situation where Eq. (7) is used for $m^*_{i,s}(\mathbf{x})$ with $w = w_p = 0.250$ mm and $w = w_p = 0.450$ mm respectively. We can see that the inner rings are less visible in Figs. 2(a) and 2(b) (especially in 2(b) where they are almost invisible) when compared to Figs. 2(c) and 2(d). This is the result of the modified Gaussian term in $m^*_{i,s}(\mathbf{x})$ being unable to suppress the Laguerre polynomial fast enough.

It has been shown in [39] that using intensity masking techniques one can in principle generate modes with very high purity (~ 0.99 for the Arrizón technique [38]) however, as can be seen in Fig. 2, that by accounting for the SMF Gaussian using the SLM hologram, the mode generated will have significantly reduced beam intensity and due to the limited contrast levels available on the SLM, the beam quality will also be reduced. We have found that the optimal w to be used in our experiment is $w \approx \frac{1}{2}w_0$.

Finally, we point out that this limitation is not intrinsic to our experiment but rather a general limitation experienced by all SPDC and back-projection experiments when intensity masking is used on the holograms. It is however not observed when azimuthal phase functions (i.e., no

#211382 - $15.00 USD Received 2 May 2014; revised 21 Jun 2014; accepted 23 Jun 2014; published 3 Jul 2014

intensity masking) are programmed to realise the standard spiral bandwidth measurements.

5. Experimental results

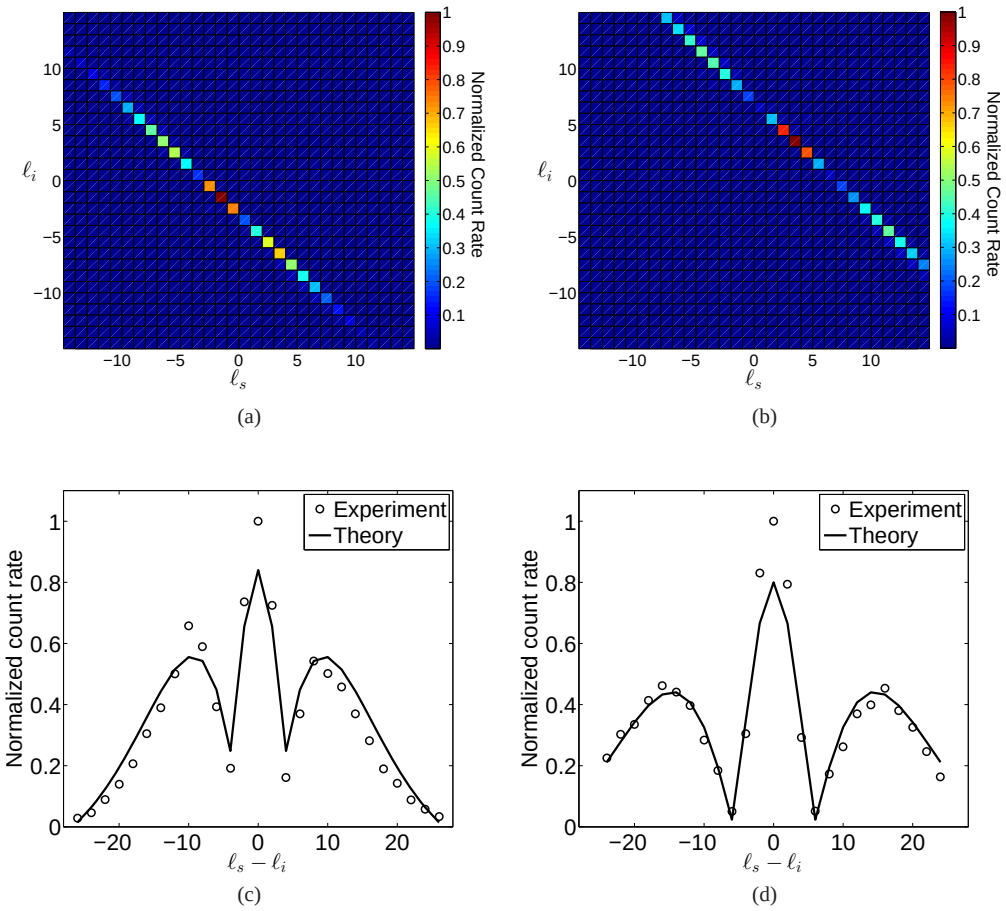

Fig. 3. Spiral bandwidth plots from the back-projection experiment for $\ell_p = -4$ and $\ell_p = 6$ is shown in (a) and (b) respectively. A cross-section along the diagonal of (a) and (b) is shown in (c) and (d) respectively with the circles representing experimental data and the solid line being the theory. Due to the high count rate of the back-projection experiment, error from the Poisson distribution of the count rate is negligible and is therefore not visible.

Figure 3 shows the spiral bandwidth plots for experiment and theory of a vortex pump in the full LG basis for $\ell_p = -4$ [Figs. 3(a) and 3(c)], and $\ell_p = 6$, [Figs. 3(b) and 3(d)], with $p_i = p_s = 0$. It can be clearly seen in Figs. 3(a) and 3(b) that the orbital angular momentum is conserved ($\ell_p = \ell_s + \ell_i$), this is consistent with that observed in [9] when a non-zero OAM pump was used in a SPDC experiment. The experimental result is compared to theory as shown in Figs. 3(c) and 3(d), we see good agreement between the two. Note that while we plot the normalized count rates the actual values are very high, ranging from a minimum of 6000 counts per second through to a maximum of 40000 counts per second. This is orders of magnitude larger than in an SPDC experiment. Consequently, the largest error in the data of Fig. 3 is

#211382 - $15.00 USD Received 2 May 2014; revised 21 Jun 2014; accepted 23 Jun 2014; published 3 Jul 2014

approximately 1% and so the error bars are negligible. An interesting feature we observed here is that in both plots the spiral bandwidth shows a narrow central peak with two broad lobes on either side, with the peak of the side lobes located at $\ell_s - \ell_i \approx 2\ell_p$ from the central maxima of the spiral bandwidth. This feature has not yet been seen in an actual SPDC experiment. An explanation as to the origin of this feature will require a more detailed theoretical investigation and is not within the scope of this paper.

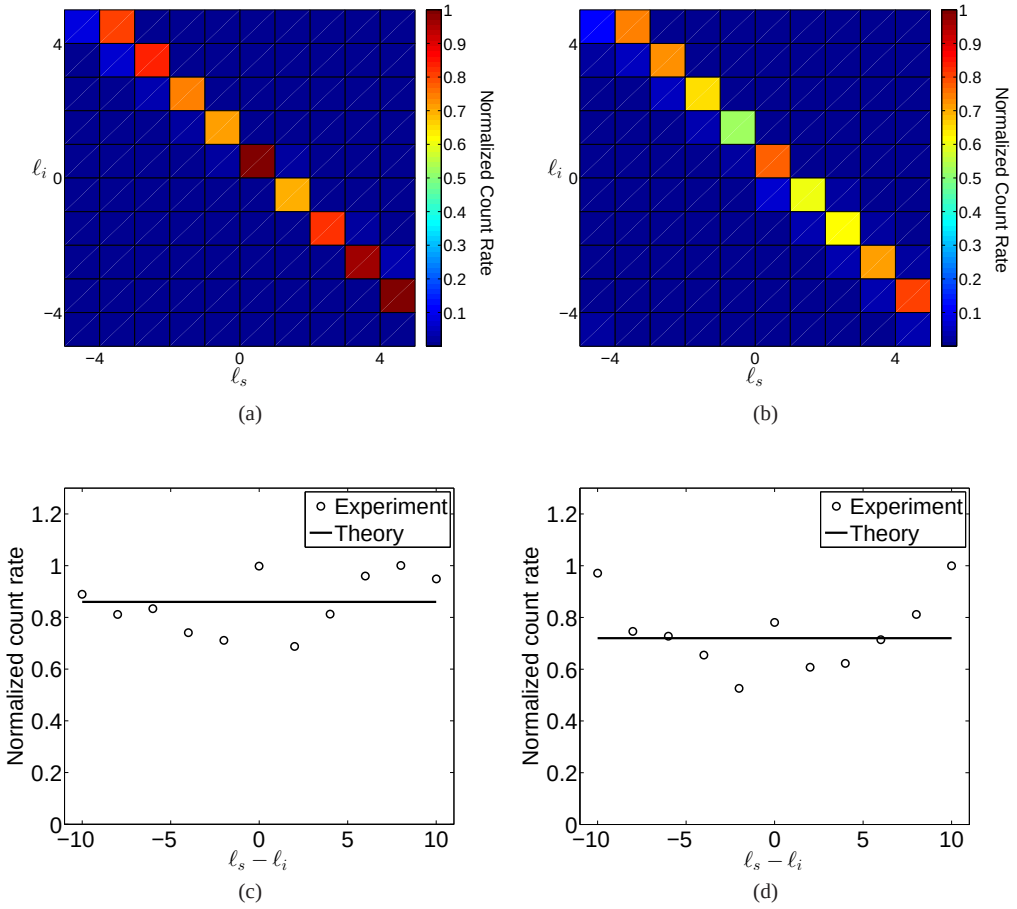

Fig. 4. Spiral bandwidth plots measured for a flat-top pump in the LG basis. (a) is measured for the radial index $p_i = p_s = 0$ and (b) is for $p_i = 3$ and $p_s = 4$, the diagonals are shown in (c) and (d) respectively with circles representing experimental data and the solid line being the theory. Due to the high count rate of the back-projection experiment, error from the Poisson distribution of the count rate is negligible and is therefore not visible.

In Fig. 4 we show the measured spiral bandwidth for a flat-top pump in the LG basis with the radial index $p_i = p_s = 0$ [Figs. 4(a) and 4(c)] and $p_i = 3$ and $p_s = 4$ [Figs. 4(b) and 4(d)]. We only show the spiral bandwidth up to $|\ell_{i,s}| = 5$, for $|\ell_{i,s}| > 5$ the quality of the beam modulated by the SLM is no longer reliable due to reasons mentioned in Section 4. We see that the measured spiral bandwidth is approximately flat, which agrees with what is expected theoretically where the spiral bandwidth is a flat curve as seen in Figs. 4(c) and 4(d). This suggests

#211382 - $15.00 USD Received 2 May 2014; revised 21 Jun 2014; accepted 23 Jun 2014; published 3 Jul 2014

that flat-top pump beams may be useful for generating high-dimensional maximally entangled states.

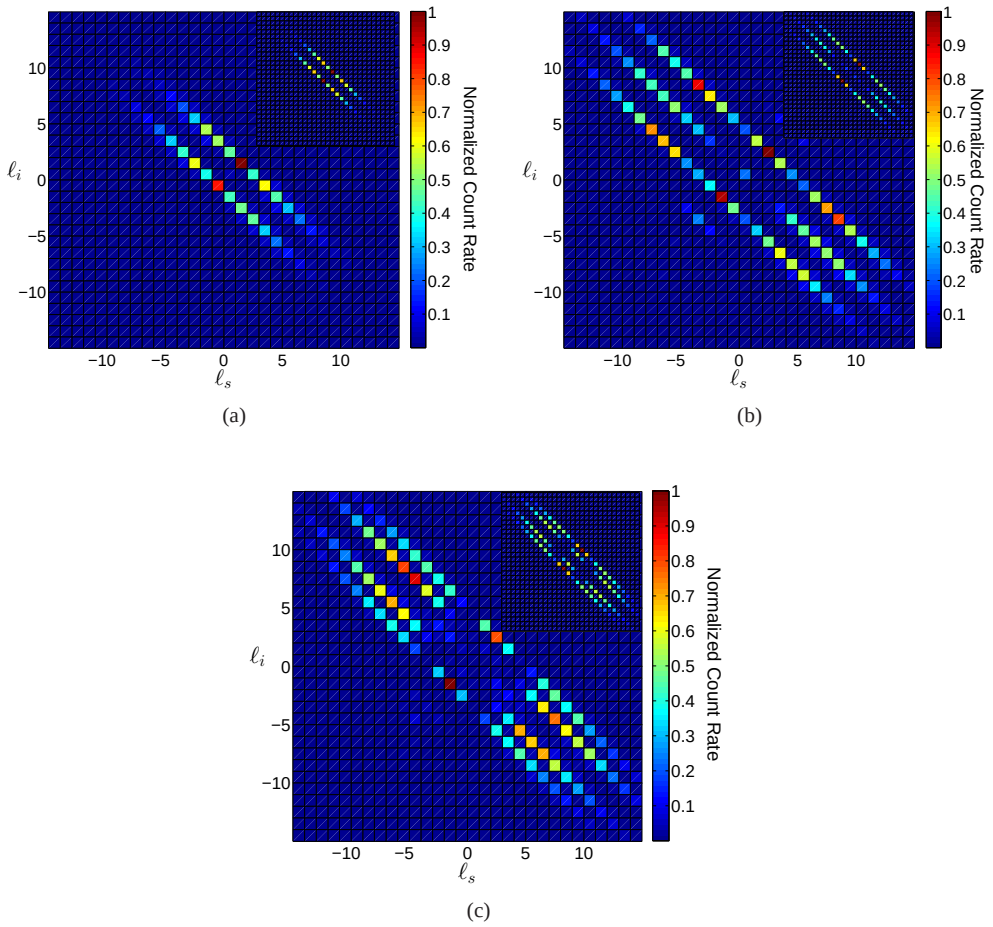

Fig. 5. Comparison of spiral bandwidth plots for experiment and theory (shown as small inset) of a HG pump in the LG basis. (a), (b) and (c) are the experimental results for a HG_{11}, HG_{22} and HG_{31} pump respectively with $p_i = p_s = 0$.

In [32] a SPDC experiment was performed with an approximation to a HG_{10} pump using a flipped Gaussian mode. We have reproduced this experiment and confirm that we obtain the same results as observed in the SPDC experiment. We also perform this experiment with our technique for a wider range of HG pump modes. Spiral bandwidth plots for a HG pump in the LG basis is shown in Fig. 5. Results for the HG_{11}, HG_{22} and HG_{31} pump with $p_i = p_s = 0$ are shown in Figs. 5(a)-5(c) respectively. Multiple bands are seen in the spiral bandwidth when using a HG pump. We can see that our experimental results agrees very well with theory.

6. Discussion and conclusion

We have demonstrated that a typical SPDC experiment with $L \ll z_R$ can be simulated with a back projection setup whereby a classical laser beam is modulated through two SLMs on

#211382 - $15.00 USD Received 2 May 2014; revised 21 Jun 2014; accepted 23 Jun 2014; published 3 Jul 2014

which the pump mode is encoded together with the signal and idler modes. Three different pump types, a vortex pump, flat-top pump and a HG pump, has been simulated with the signal and idler beams in the LG mode.

For the vortex pump we have shown that there is good agreement between theory and experiment. We indeed see conservation of angular momentum as observed in [9]. We also observed in the spiral bandwidth a narrow central peak with two broad lobes on either side located at $\ell_s - \ell_i \approx 2\ell_p$ from the central peak, which we predict will be observed in future SPDC experiments.

The spiral bandwidth generated from a simulated flat-top pump shows good agreement with theory for $|\ell_{i,s}| < 5$ however for larger $\ell_{i,s}$ the measured count rate drops too low to be reliable.

For the HG pump there is generally good agreement between theory and experiment for HG modes with *n* and *m* less than 3. At large HG modes the resulting OAM spectrum becomes much more complicated and our current setup does not have the accuracy to resolve some of the finer details in the OAM spectrum. We observe multiple bands in the spiral bandwidth for a HG pump, this is in agreement with [32].

The major advantages of using a back projection setup is that it can obtain photon count rates many orders of magnitude larger than that for a typical down conversion experiment thereby giving much better accuracy. The back projection setup is not as sensitive to alignment compared to a down conversion experiment, this allows it to be set up in a relatively short time and be used to give a preview on whether a down conversion experiment will be feasible or not. Lastly one can turn a back projection setup into a down conversion setup simply by changing two of its components.

Our results also hint at a major source of uncertainty in future SPDC experiments when the full LG basis is used for the post-selected state: there is significant loss of beam quality and count rate due to the need to cancel the SMF mode Gaussian contribution by modifying the SLM holograms. We suggest that it should be possible to correct for this issue by using a Gaussian to top-hat beam converter at the entrance to the SMF.

#211382 - $15.00 USD Received 2 May 2014; revised 21 Jun 2014; accepted 23 Jun 2014; published 3 Jul 2014